RESEARCH PAPER

Synthesis, Characterization, and Anticancer Evaluation of a Novel Imine-Oxime Ligand Derived from 2-Hydrazinyl Benzothiazole and Its Palladium(II) Complex

Najlaa Nouri Nejm *, Hayder Obaid Jamel

Department of Chemistry, College of Education, University of Al-Qadisiyah, Diwaniyah, Iraq

ARTICLE INFO

Article History:
Received 19 March 2025
Accepted 12 June 2025
Published 01 July 2025

Keywords:
Anticancer
Benzothiazole
Metal complexes
Oxime

ABSTRACT

The nano ligand, (2E,3E)-3-((4-((E)-1-(2-(benzo[d]thiazol-2-yl) hydrazineylidene) ethyl)phenyl) imino) butan-2-one oxime (BTHEPIBO), was synthesized in three steps. The first stage produced 2-hydrazineylbenzothiazole by reacting 2-mercaptobenzothiazole with hydrazine hydrate in ethanol. Second, a few drops of glacial acetic acid catalyzed the reaction of 4-aminoacetophenone with diacetyl monoxime in ethanol. In the last step, the two intermediate products formed nano BTHEPIBO ligand. The reaction with palladium (II) chloride produced a palladium (II) complex of this nano ligand. FT-IR, ^{1}H-NMR, UV-Vis, melting point determination, FESEM, XRD, and magnetic susceptibility measurements were used to determine the chemical structures of the nano ligand and its palladium complex. The synthesized nano ligand and palladium (II) complex were tested for their impact on MCF-7 breast cancer cell proliferation. The nano ligand and its combination inhibited cancer cell multiplication, suggesting possible use in cancer treatment. This paper shows the effective synthesis and complete characterization of a novel nano ligand and its complex, as well as their intriguing biological properties, paving the path for medicinal chemistry research.

How to cite this article
Nejm N., Jamel H. Synthesis, Characterization, and Anticancer Evaluation of a Novel Imine-Oxime Ligand Derived from 2-Hydrazinyl Benzothiazole and Its Palladium(II) Complex. J Nanostruct, 2025; 15(3):962-973. DOI: 10.22052/JNS.2025.03.014

INTRODUCTION

Heterocyclic benzothiazole has a benzene ring fused with a thiazole ring [1]. The thiazole ring has carbon, hydrogen, nitrogen, and sulphur atom [2, 3]. As a weak base, benzothiazole is a colorless liquid with low viscosity, 1.238 g/mL density, and 227-228°C boiling point [4]. It is a precursor of Schiff-bases, azo dyes, and other chemical molecules [1]. Biological, analytical, and organic fields use benzothiazole and its derivatives [5]. Benzothiazole's thioamide functional group makes it biologically effective. This chemical is anticancer, antibacterial, antifungal, and antiviral, and its derivatives are anti-inflammatory and analgesic [6, 7]. Benzothiazole suppresses hunger and is found in tea leaves and blackberries [8]. Hofmann originally synthesized benzothiazole in 1887, and many methods have been developed for its derivatives [9]. Benzothiazole and its derivatives display considerable potential in coordination chemistry for synthesis of metal complex. Coordination compounds with nitrogen and sulphur donor atoms are fascinating due to their chemical, physical, biological, and pharmacological

* Corresponding Author Email: *chem.edu.post17@qu.edu.iq*

properties [10-13]. The metal ions involved in many biological processes are coordinated by nitrogen and sulphur atoms [14]. Coordinating the biologically active chemical with a transition metal ion usually boosts activity [15]. R1R2C=NOH is the conventional formula for an imine oxime. R1 can be hydrogen for an aldoxime or ketoxime, and R2 can be an organic side chain [16-20]. A reductive amination reaction between hydroxylamine hydrochloride and an alcoholic carbonyl solution produces oximes [21]. This synthesis reaction is crucial to organic chemistry for several uses [22-25]. Ketones and primary amines generate imines (C=NR) by removing water. The chemical process involves adding hydroxylamine to the carbonyl group to generate an unstable hemiacetal intermediate, which rapidly loses a water molecule to form an oxime with the C=N group [26]. Oximes have anticonvulsant, antibacterial, antioxidant, anticancer, depressive, and antiviral effects [27]. Oxime coordination chemistry can separate, purify, and remove metal ions [28]. These complexes produces the structural models for biological systems like vitamin B_{12} and have considerable anticancer activity [28]. Oximes coordinate via nitrogen, oxygen, and/or both [29].

In our study, the nano ligand containing the benzothiazole ring and its palladium(II) complex were synthesized. The techniques employed for characterization included FTIR, ^{1}H-NMR, UV-Vis spectra, FESEM, and CHNS analysis. Additionally, the biological activity of the synthesized compounds was evaluated using the MTT assay to assess their potential as anticancer agents.

MATERIALS AND METHODS

Materials and instruments

This study used various high-purity chemical components from BDH, Aldrich, Merck, and HIMEDIA. A Shimadzu UV-165PCS spectrophotometer was used to acquire UV-Vis. spectra in the 200-1000 nm area with a concentration of 1×10^{-3} M, ethanol solvent, and a 1 cm absorption cell. A Varian Fourier Transform device was used to capture ^{1}H-NMR spectra at 300 MHz using DMSO-d6 as the solvent and tetramethyl silane as the internal standard reference. FTIR spectra were taken using a Shimadzu FTIR 8400S spectrophotometer in the 400-4000 cm^{-1} range. Scientists used stuart melting point device to determine chemical melting points. Room-temperature susceptibility was tested with the MSB-MKI magnetic susceptibility balance. A Shimadzu AA-6300 atomic absorption flame spectrophotometer measured the complexes' metal content, and an EA-300.mth elemental analyzer performed CHNS. The synthesized chemicals were investigated using a Czech MIRA3 TESCAN field emission scanning electron microscope (FESEM). X-ray diffraction (XRD) measurements were taken using the 20-80 degree D2 Phaser Bruker AXS GmbH. A Digital Conductivity Series Ino. Cond 3110 SET1 measured electrical conductivity at 1×10^{-3} M concentration in ethanol a solvent at room temperature.

Preparation of the nano BTHEPIBO ligand

The BTHEPIBO ligand was prepared by the following steps (See Fig. 1):

Preparation of compound (A)

2-Hydrazineylbenzothiazole (Compound-A) was synthesized by reacting 2-mercaptobenzothiazole (1.67 g, 0.01 mol) dissolved in 25 mL of absolute ethanol in a round-bottom flask. A solution containing 5 mL of hydrazine hydrate and 15 mL of absolute ethanol was added to the mixture with continuous stirring, and the reaction mixture was refluxed for 8 h at 78°C. The reaction was monitored by the blackening of lead acetate paper. The solution was then cooled at room temperature, filtered, and the resulting precipitate was collected. The precipitate was recrystallized from hot absolute ethanol to remove any unreacted residues, dried, and collected, yielding a 69% product with a melting point of 90-98°C.

Preparation of compound (B)

The synthesis of (E)-1-(4-((2-hydroxy-1,2-diphenylethylidene) amino) phenyl) ethan-1-one (Compound-B) was achieved by dissolving 4-aminoacetophenone (1.35 g, 0.01 mol) in 25 mL of absolute ethanol in a round-bottom flask. After that, diacetyl monoxime (1.01 g, 0.01 mol) dissolved in 25 mL of absolute ethanol and 5-6 drops of glacial acetic acid were added. The mixture was refluxed for 8 h. The precipitate was filtered, dried, and recrystallized from absolute ethanol, yielding an 82% product with a melting point of 98-100°C.

Preparation of the nano BTHEPIBO ligand

The BTHEPIBO ligand was synthesized by dissolving 1.65 g (0.01 mol) of compound (A) in 25 mL of absolute ethanol under continuous stirring. A solution of 2.18 g (0.01 mol) of compound (B), dissolved in 15 mL of absolute ethanol, was added, along with 5-6 drops of glacial acetic acid. The mixture was refluxed for 8 h, cooled, and resulted in the formation of a precipitate. After filtration, drying, and recrystallization from absolute ethanol, the yield was 73%, with a melting point of 113-115°C.

Preparation of palladium (II) complex

The palladium (II) complex of the BTHEPIBO ligand was synthesized by dissolving 0.365 g (0.001 mol) of the BTHEPIBO ligand in 25 mL of absolute ethanol. A solution was separately prepared by dissolving 0.180 g (0.001 mol) of palladium (II) chloride in 25 mL of absolute ethanol, which was then added to the nano ligand solution. The mixture was refluxed with stirring for 2 h.

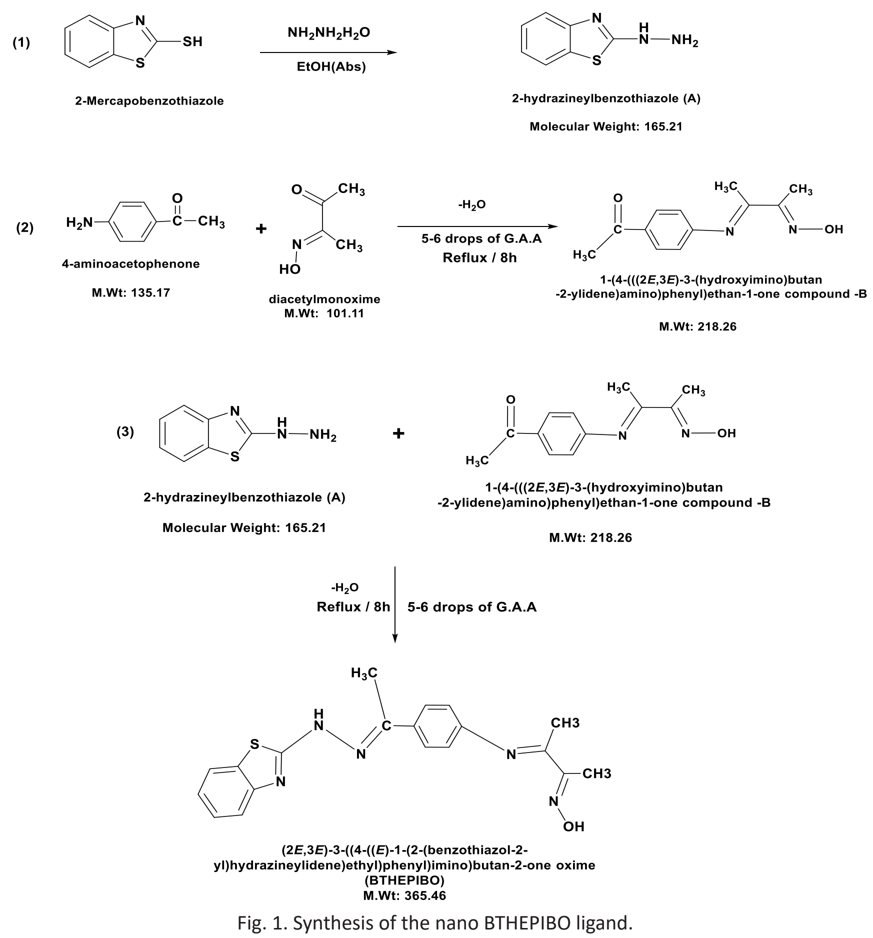

Fig. 1. Synthesis of the nano BTHEPIBO ligand.

Table 1. Physical properties of the prepared BTHEPIBO ligand and its complexes.

Compound (Chemical formula)	Color	M.P (°C)	Yield %	Mol. Wt. (g/mol)	Calc. (Found)%				
					C	H	N	S	Pd
Nano ligand (BTHEPIBO) $C_{19}H_{19}N_5OS$	Dark Yellow	113-115	73	365.46	62.45 (63.12)	5.24 (5.31)	19.16 (19.65)	8.76 (8.98)	----- -----
[Pd(BTHEPIBO)Cl]Cl $C_{19}H_{19}Cl_2N_5OPdS$	Reddish Brown	175-177	79	542.78	42.04 (42.63)	3.53 (3.59)	12.90 (13.34)	5.91 (6.17)	19.61 (19.94)

Precipitates was filtered, dried, and recrystallized from absolute ethanol. This process yielded a colored and pure precipitate of the metal complex with a yield of 79% and a melting point of 175-177°C. The physical properties of samples have been listed in Table 1.

MTT test

The cytotoxicity of the new BTHEPIBO ligand and its palladium (II) complex was evaluated over MCF-7 breast cancer cells and the normal HEK-293 cell line to assess their efficacy as anticancer agents. Firstly, the cancer cell lines were prepared, and cell suspensions were distributed into a 96-well flat-bottom plate, followed by incubation in a 5% CO_2 atmosphere at 37°C for 24 h. Subsequently, 100 µL of the cell suspension were added to each well, along with varying concentrations of the studied compounds (5, 10, 25, 50, 100, 250, 500 µg/mL), each in triplicate. The plate was then further incubated for 24 h at 37°C. After the incubation period, 10 mL of a 3-(4,5-dimethylthiazol-2-yl)-5-(3-carboxymethoxyphenyl)-2-(4-sulfophenyl)-2H-tetrazolium bromide solution at a concentration of 0.5 mg/mL was added to each well. The plate was incubated for an additional 4 h at 37°C. To dissolve the crystals, 100 µL of a solubilization solution were added, and the absorbance of the samples was measured at a wavelength of 570 nm using a microplate reader (DNM - 9602G). The absorbance values were used to determine cell viability, expressed as a percentage relative to untreated cells, indicating the number of viable cells in the medium after treatment with the compounds.

RESULTS AND DISCUSSION

The BTHEPIBO ligand was introduced as dark yellow crystals, whereas its palladium (II) complex appears reddish-brown. Both the nano ligand and its complex demonstrated good solubility in various solvents such as ethanol, methanol, DMSO, and DMF, but they are insoluble in distilled water and ether. The molar ratio for preparing the palladium complex was determined using the molar ratio method, as described by June [30]. This method involves preparing the solutions of equal concentrations of the ligand and the metal ion, with employing different volumes of the nano ligand. Absorbance measurements are taken at appropriate wavelengths for each case. The relationship between the resulting absorbance and the molar ratio (VL/VM) is plotted, revealing a ratio of the complex as 1:1 (metal to nano ligand ratio). Additionally, the ionic nature of the prepared complex was assessed by measuring its molar conductivity using ethanol as the solvent at room temperature and a concentration of 1×10^{-3} M. The palladium (II) complex exhibited good molar conductivity, indicating an ionic character with a 1:1 metal to nano ligand ratio, with a measured conductivity value of 38.18 ohm^{-1} cm^2 mol^{-1}.

^{1}H-NMR results

The ^{1}H-NMR spectrum was studied using a Varian Fourier Transform instrument operating at a frequency of 300 MHz, as displayed in Fig. 2. Tetramethylsilane served as the internal standard,

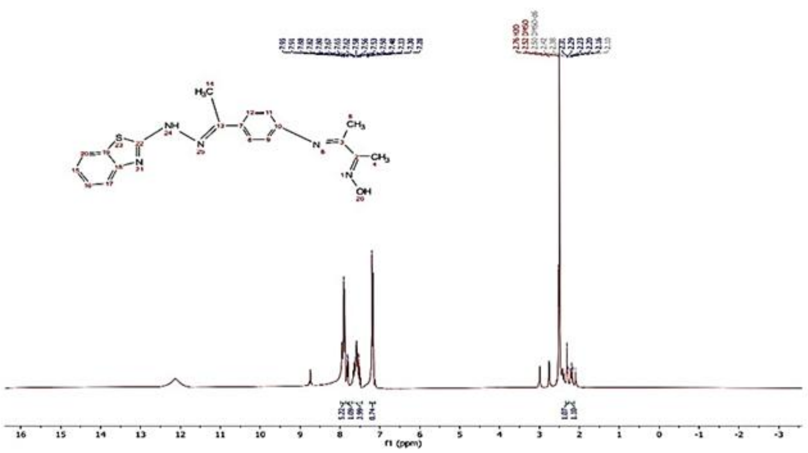

Fig. 2.^{1}H-NMR spectrum of the prepared BTHEPIBO ligand.

and DMSO-d_6 was used as the solvent at room temperature. The ^{1}H-NMR spectrum of the BTHEPIBO ligand displayed a singlet at a chemical shift (s, 3H, δ = 2.31 ppm), corresponding to the protons of the methyl group ($-C=N-CH_3$). A singlet at s, 3H, δ = 2.10 ppm was observed, indicating the protons of the methyl group attached to the oxime group [31]. The protons of the methyl group linked to the imine group produced a singlet at s, 3H, δ = 2.98 ppm [32]. Multiple signals were detected within the range of M, 8H, δ = 7.28 - 8.82 ppm, representing the aromatic ring protons [33]. Additionally, singlet signals at S, 1H, δ = 8.74 ppm and S, 1H, δ = 12.16 ppm were attributed to the protons of the secondary amine (-NH) group and the hydroxyl group of the oxime, respectively [34]. The singlet at 2.52 ppm was due to the protons of the DMSO-d_6 solvent.

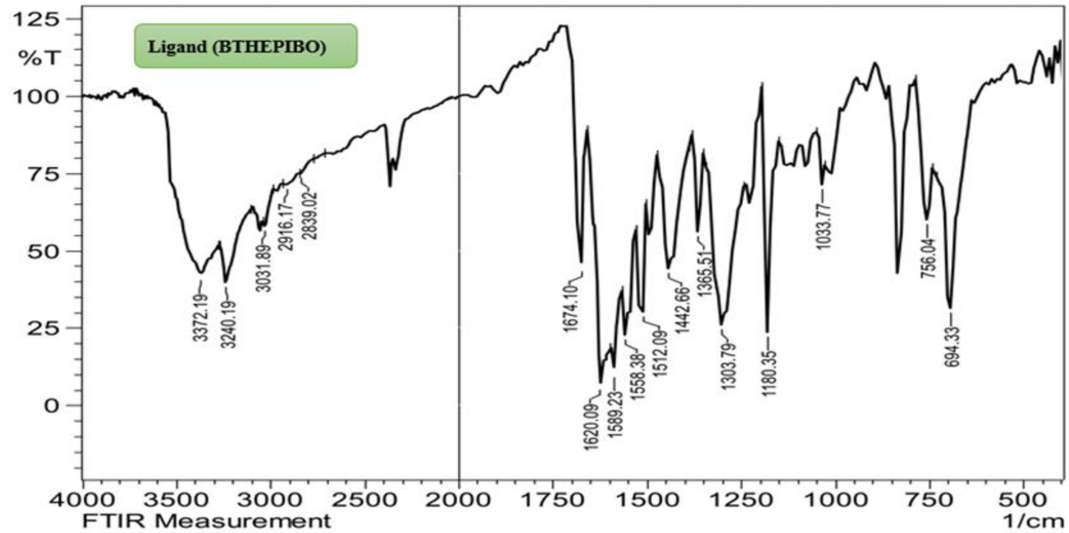

Fig. 3. FTIR spectrum of BTHEPIBO ligand.

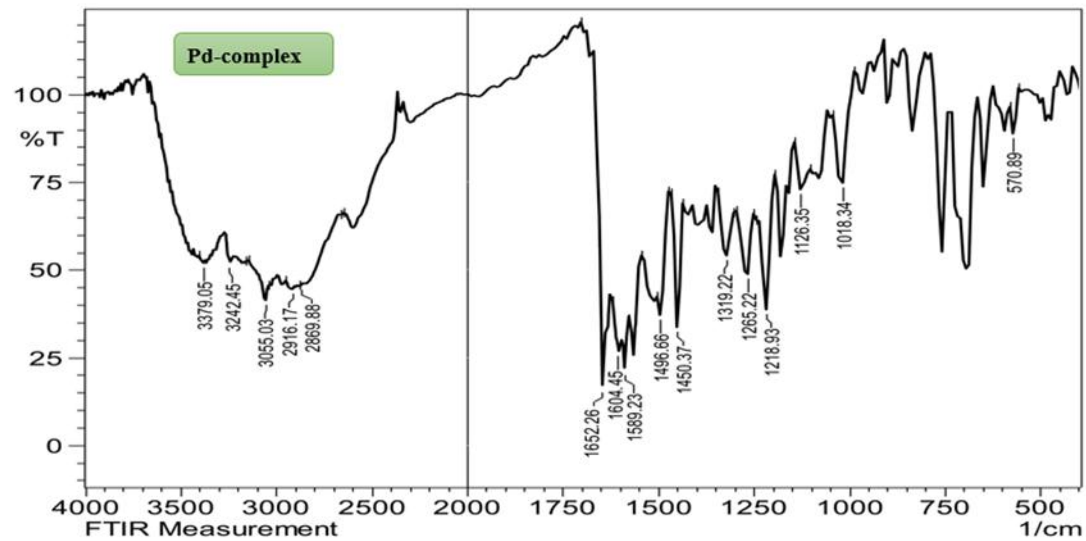

Fig. 4. FTIR spectrum of the palladium (II) complex.

FT-IR results

To obtain the FTIR spectrum of the samples, potassium bromide was utilized. The spectrum of the free nano ligand in Fig. 3 exhibited two distinct absorption bands at 3372 and 3240 cm^{-1}, corresponding to the hydroxyl group of the oxime and the secondary amine υ(N-H), respectively [35-37]. An absorption band at 1674 cm^{-1} was observed, indicating the azomethine group (C=N) of the Schiff base, thereby confirming the formation of the nano ligand [38]. Distinct bands at 1620 and 1589 cm^{-1} were attributed to the azomethine groups of the oxime and the benzothiazole ring, respectively [39]. The C=C and C-H groups of the aromatic rings in the nano ligand are appeared at 1558, 1455, and 3031 cm^{-1}, respectively. Additionally, a band at 1033 cm^{-1} indicated the presence of the υ(C-S) functional group of the benzothiazole ring [40, 41]. The FTIR spectrum of the synthesized palladium (II) complex is shown in Fig. 4. The Schiff base's azomethine group shifted to a lower frequency than that of the free nano ligand spectrum. It was centered at 1674 cm^{-1} in the free nano ligand and displaced as 1652 cm^{-1} in the produced complex spectrum [42-46]. A decrease in the azomethine group's frequency of the oxime was noticed

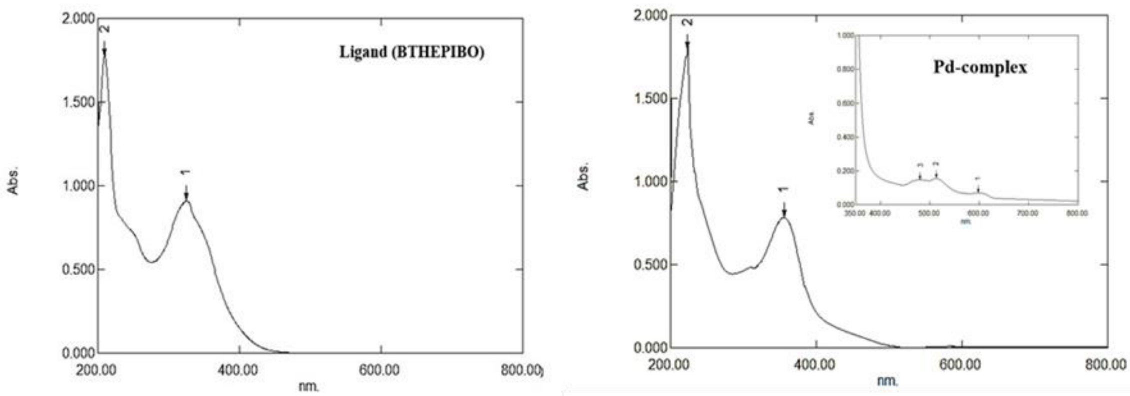

Fig. 5. UV–Vis spectra of BTHEPIBO ligand and its palladium (II) Complex.

Table 2. Spectral bands of BTHEPIBO ligand and palladium (II) complex.

Compound	υ (O-H) Oxime υ (N-H) 2^0Amine	υ (C-H) Aromatic	υ(C=N) Imine υ(C=N) Oxime	υ(C=N) Benzothiazole	υ(C=C) aromatic	υ(M-N)
Nano ligand (BTHEPIBO)	3372 3240	3031	1674 1620	1589	1558 1442	-
[Pd(BTHEPIBO)Cl]Cl	3379 3245	3055	1652 1604	1589	1566 1450	570

Table 3. UV-Visible absorption peaks, magnetic momentum and expected geometry of ligand (BTHEPIBO) and its palladium (II) Complex.

Compounds	λ (nm)	υ⁻ (cm^{-1})	Transitions	μeff (B.M)	Geometry
Nano ligand (BTHEPIBO)	212 324	47170 30864	π-π* n-π*	–	–
[Pd(BTHEPIBO)Cl]Cl	223 354 482 514 598	44843 28249 20747 19455 16722	Intra Nano ligand Intra Nano ligand $^1A_1g \rightarrow {}^1Eg$ $^1A_1g \rightarrow {}^1B_1g$ $^1A_1g \rightarrow {}^1A_2g$	(Dia.)	Square planar dsp^2

around 1604 cm^{-1} in the spectrum of the prepared compound. These changes strongly suggest that the nitrogen atoms of the azomethine groups coordinate the nano ligand with the palladium ion. The complex spectrum showed a new band at 570 cm^{-1}, indicating the presence of a metal-nitrogen (M-N) group (See Table 2) [47].

UV–Vis spectra

Solutions of metal complex compounds have distinctive colors due to their absorption in the visible region of the spectrum, in addition to other absorptions in the ultraviolet region because they contain partially filled secondary (d) levels with electrons [48]. The UV-visible spectrum of the BTHEPIBO ligand in Fig. 5 shows two distinct absorption peaks at 212 nm (47170 cm^{-1}) and 324 nm (30864 cm^{-1}). The first peak indicates the π-π* transition, while the second peak indicates the n-π* transition of the azomethine (C=N) group [49]. The spectrum of the palladium (II) complex in Fig. 5 shows new absorption peaks that were not present in the free Nano ligand's spectrum. In addition to the peaks at 223 nm (44843 cm^{-1}) and 354 nm (28249 cm^{-1}), which all indicate intra ligand transitions, new absorption peaks are appeared at 482 nm (20747 cm^{-1}), 514 nm (19455 cm^{-1}), and 598 nm (16722 cm^{-1}), corresponding to the electronic transitions $^1A_1g \rightarrow {}^1Eg$, $^1A_1g \rightarrow {}^1B_1g$, and $^1A_1g \rightarrow {}^1A_2g$, respectively. The presence of these transitions confirms that the complex has a square planar geometry. Magnetic susceptibility measurements performed on the complex, which gave values close to zero, proved that all electrons in the secondary (d) shell are paired (See Table 3) [50].

XRD analysis

A study of the crystal structures of both the nano BTHEPIBO ligand and its palladium (II) complex was conducted using XRD measurement in Fig. 6. The XRD data provided valuable information about the crystal structure, crystal volume, and purity of the prepared compounds [51-53]. Analysis of the XRD patterns revealed that the presence of sharp peaks indicates the formation of a crystalline lattice, confirming that the compound exhibits a crystalline or semi-crystalline nature. However, if

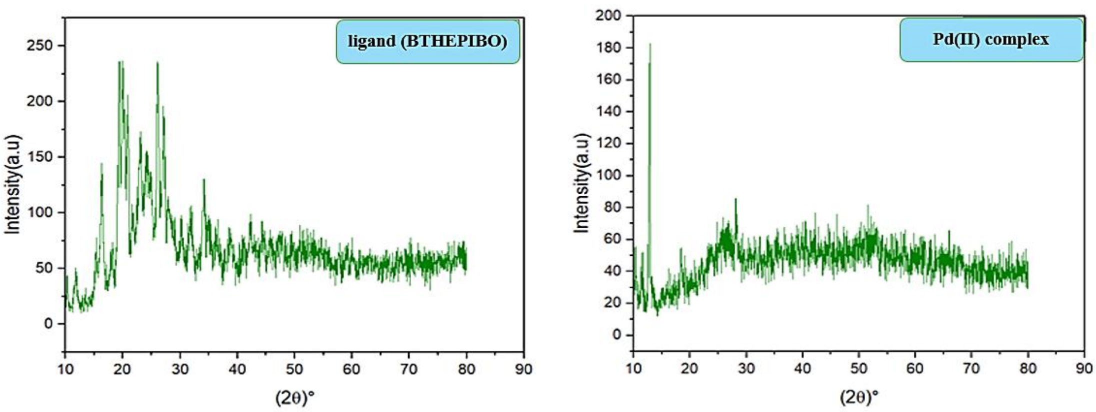

Fig. 6. XRD patterns of the nano BTHEPIBO ligand and its palladium (II) complex.

Table 4. Summary of the information obtained from the XRD analysis i.e., diffraction angles, d-spacing, and relative intensities for nano BTHEPIBO ligand and its palladium (II) complex.

Compound	No.	Peak Position °2θ	Peak Width (FWHM)	Crystallite size(nm)	Rel. Int [%]	Lattice Strain
Nano ligand (BTHEPIBO)	1	26.106	0.514	16.58	100	0.0097
	2	19.274	0.409	20.59	92	0.0100
	3	27.070	0.539	15.84	80	0.0098
[Pd(BTHEPIBO)Cl]Cl	1	12.798	0.430	19.43	100	0.0167
	2	26.464	4.639	1.83	64.46	0.0861
	3	42.888	0.183	48.73	52.81	0.0029

the peaks appear broad and not sharp, it indicates that the compound is non-crystalline [54]. The Debye-Scherrer equation was used to calculate the crystallite sizes for the BTHEPIBO ligand and the palladium complex.

Analysis of the XRD patterns revealed distinct differences in crystallite size, dislocation density, and interplanar spacing (d) between the nano ligand and the prepared palladium (II) complex. These differences confirm the coordination process between the nano ligand and the palladium (II) ion, as detailed in Table 4. The data obtained from the XRD measurements indicate that the prepared materials possess a nanoscopic nature [32].

FESEM analysis

Using SEM analysis, detailed information about the surface morphology, particle size, and shape of both samples was obtained [55]. FESEM measurement was employed with a scale of 200 nm and a magnification power of (Mag = 135KX). As depicted in Fig. 7, analysis of the FESEM images of the nano ligand (BTHEPIBO) revealed small, agglomerated, non-homogeneous spherical particles with an average particle size of 36.65 nm. In contrast, the FESEM image of the palladium (II) complex showed very small, unevenly distributed spherical granules with an average particle size of 29.88 nm [56].

Effect of the BTHEPIBO ligand on the growth of breast cancer (MCF-7) and normal (HEK) cell lines

The study on the effect of the BTHEPIBO ligand on the growth of the MCF-7 breast cancer cell

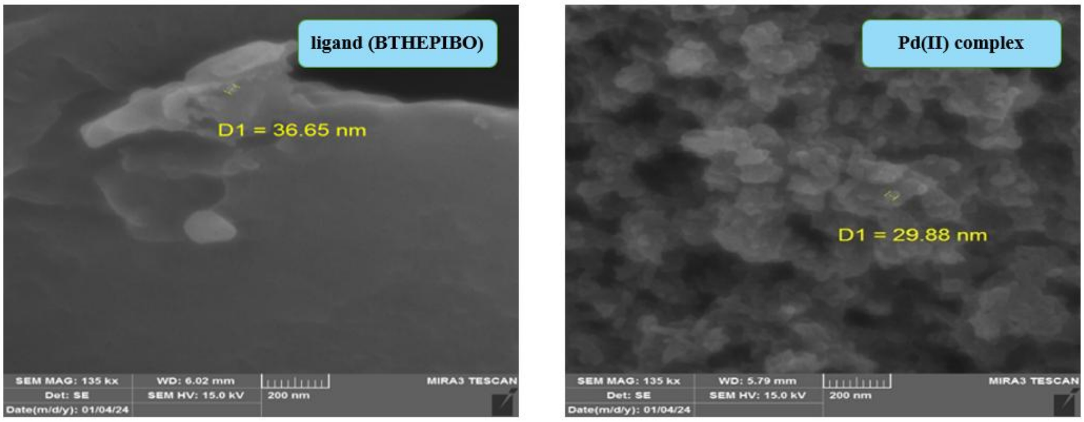

Fig. 7. FE-SEM images of BTHEPIBO ligand and its palladium (II) complex.

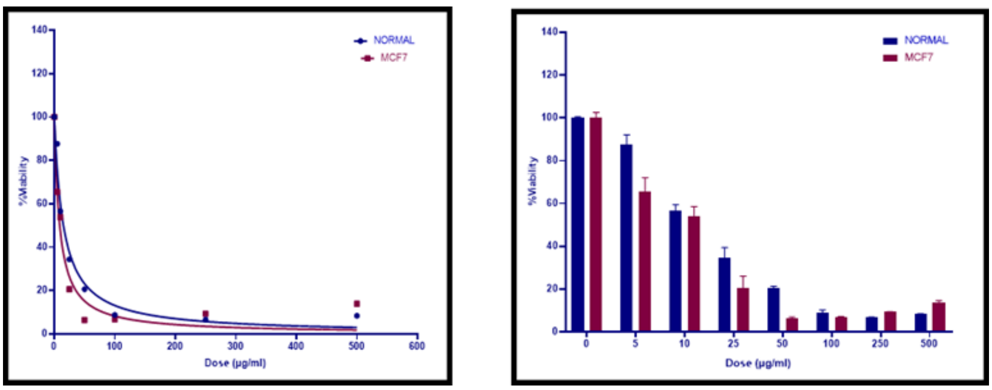

Fig. 8. Comparison of viable cells at selected concentrations for the breast cancer cell line MCF-7 and the normal cell line HEK by employing the nano BTHEPIBO ligand.

line revealed a low inhibition rate at the lowest concentration of 5 µg/mL, where the inhibition rate of breast cancer cell growth was 34.10%. In contrast, the lowest inhibition rate for the growth of normal HEK cells at the same concentration was 12.34%. However, at a concentration of 50 µg/mL, the ligand exhibited a significantly higher inhibition rate, with the growth inhibition of breast cancer

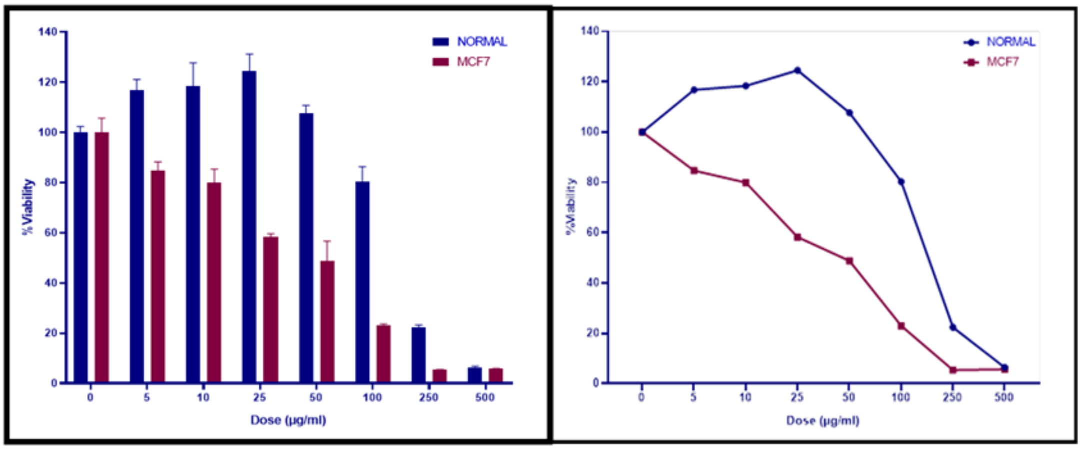

Fig. 9. Comparison of viable cells at selected concentrations for the breast cancer cell line MCF-7 and the normal cell line HEK by employing the palladium (II) complex.

Table 5. Effect of the nano BTHEPIBO ligand on the cancer cell line of breast cancer MCF-7 and its comparison with the normal cell line Hek-293 at the same concentration using the MTT assay for 24 h.

Conc. µg/mL	Cancer cell MCF-7			Normal cell Hek-293		
	Cell Viability		Cell Inhibition %	Cell Viability		Cell Inhibition %
	Mean	SD		Mean	SD	
0	100	0	0	100	0	0
5	65.90	4.09	34.1	87.66	4.35	12.34
10	18.83	3.46	81.17	56.53	2.89	43.47
25	5.21	0.11	94.79	34.37	4.99	65.63
50	5.86	0.20	94.14	20.61	0.70	79.39
100	6.48	0.30	93.52	8.70	1.45	91.3
250	7.33	0.76	92.67	6.57	0.28	93.43
500	8.44	0.69	91.56	8.30	0.11	91.7
IC50	8.09			28.68		

Table 6. Effect of the palladium (II) complex of the BTHEPIBO ligand on the MCF-7 breast cancer cell line and comparison with the normal Hek-293 cell line at the same concentration using the MTT assay for 24 h.

Conc. µg/mL	Cancer cell MCF-7			Normal cell Hek-293		
	Cell Viability		Cell Inhibition %	Cell Viability		Cell Inhibition %
	Mean	SD		Mean	SD	
0	100	0	0	100	2.439	0
5	84.67	3.620	15.33	116.78	4.294	16.78
10	79.94	5.423	20.06	118.36	9.407	18.36
25	58.26	1.369	41.74	124.55	6.737	24.55
50	48.85	7.905	51.15	107.73	3.049	7.73
100	23.02	0.672	76.98	80.31	5.995	19.69
250	5.39	0.146	94.61	22.40	0.821	77.6
500	5.68	0.221	94.32	6.45	0.410	99.59
IC50	35.91			218.4		

cells reaching 94.14%. The highest inhibition rate for the growth of normal HEK cells was observed at a concentration of 250 µg/mL, peaking at 93.43%. The best inhibition rate for breast cancer cells at 50 µg/mL was 94.14%, while the inhibition rate for the normal cell line at the same concentration was 79.39%. The inhibition rate of normal cell growth can be reduced by modifying the ligand. Based on the obtained results, the half-maximal inhibitory concentration (IC50) of the ligand against the breast cancer cell line was 8.09 µg/mL, while the IC50 for normal HEK cells was 28.68 µg/mL. These findings suggest that the BTHEPIBO ligand is a promising candidate for breast cancer treatment [57], as shown in Table 5 and Fig. 8.

Effect of the palladium (II) complex on the growth of breast cancer (MCF-7) and normal (HEK) cell lines

When studying the effect of the palladium (II) complex of the BTHEPIBO ligand on the growth of the MCF-7 breast cancer cell line, the complex showed a low inhibition rate at a concentration of 5 µg/mL, where the inhibition rate of the growth of the breast cancer cell line was 15.33%. Meanwhile, the lowest inhibition rate for the growth of normal (HEK) cells was observed at a concentration of 50 µg/mL, showing an inhibition rate of 7.73%. However, it showed a higher inhibition rate at a concentration of 250 µg/mL, where the inhibition rate of the growth of breast cancer cells was 94.61%. The inhibition rate for the growth of normal (HEK) cells at the same concentration was 77.60%. Based on the obtained results, the half-maximal inhibitory concentration (IC_{50}) of the complex against the breast cancer cell line was 35.91 µg/mL, while the (IC_{50}) for normal (HEK) cells was 218.4 µg/mL, as shown in Table 6 and Fig. 9. By comparing the results of the study of both BTHEPIBO ligand and its palladium(II) complex, a similarity in the results was found, which suggests a wide potential for treatment [58].

CONCLUSION

This study involved the synthesis of the novel imine-oxime ligand derived from 2-hydrazinylbenzothiazole, along with its palladium (II) complex. Various spectroscopic and physical methods were employed to elucidate the structures of both the ligand and its palladium (II) complex. FTIR data confirmed the formation of azomethine groups, which shifted to lower frequencies upon coordination, indicating the formation of metal complexes. This technique also demonstrated that the nano ligand coordinates with the palladium (II) ion through the nitrogen atoms of the azomethine groups of the Schiff base and the oxime azomethine group, confirming the tridentate nature of the nano ligand. Additionally, the UV-visible spectrum of the palladium (II) complex revealed a square planar geometry. Molar conductivity measurements indicated that the palladium (II) compound possesses an ionic nature. Furthermore, FESEM and XRD measurements showed that the palladium (II) complex has a nanoscale size. The MTT assay was utilized to investigate the potential use of the nano ligand and its palladium (II) complex as anticancer agents against the MCF-7 breast cancer cell line. Both compounds demonstrated significant activity against the cell lines used in the study.

CONFLICT OF INTEREST

The authors declare that there is no conflict of interests regarding the publication of this manuscript.

REFERENCES

1. Zhou L, Xu Z, Hua C, Cao H, Qin B, Zhao H, et al. Facile synthesis of nitrogen and sulfur co-doped hollow microsphere polymers from benzothiazole containing wastewater for water treatment. Chemosphere. 2022;287:131982.
2. Patil P, Virupaxappa SB, Latha MS, Shridhar AH. Synthesis, Structural Characterization Of Benzothiazole Schiff Base Metal (II) Complexes And Their Interaction With DNA. Journal of Pharmaceutical Negative Results. 2022:466-472.
3. Gill RK, Rawal RK, Bariwal J. Recent Advances in the Chemistry and Biology of Benzothiazoles. Arch Pharm. 2015;348(3):155-178.
4. Singh C, Kumar R, Mazumder A, Salahuddin, Kumar A, Sahu R, et al. Benzothiazole: Synthetic Strategies, Biological Potential, and Interactions with Targets. Mini Rev Org Chem. 2022;19(2):242-256.
5. Soni B, Ranawat MS, Sharma R, Bhandari A, Sharma S. Synthesis and evaluation of some new benzothiazole derivatives as potential antimicrobial agents. Eur J Med Chem. 2010;45(7):2938-2942.
6. Synthesis of 2-Substituted Benzothiazole Derivatives and Their In Vitro Anticancer Effects and Antioxidant Activities Against Pancreatic Cancer Cells. Anticancer Res. 2017;37(11).
7. Monsef R, Soofivand F, Abbas Alshamsi H, Al-Nayili A, Ghiyasiyan-Arani M, Salavati-Niasari M. Sonochemical synthesis and characterization of PrVO4/CdO nanocomposite and their application as photocatalysts for removal of organic dyes in water. J Mol Liq. 2021;336:116339.
8. Wazzan N, Safi Z, Al-Barakati R, Al-Qurashi O, Al-Khateeb L. DFT investigation on the intramolecular and intermolecular

proton transfer processes in 2-aminobenzothiazole (ABT) in the gas phase and in different solvents. Struct Chem. 2019;31(1):243-252.
9. Franklin EC. The Hofmann-Beckmann-Curtius-Lossen Rearrangements. Chem Rev. 1934;14(2):219-250.
10. Joseph J, Boomadevi Janaki G. Synthesis, structural characterization and biological studies of copper complexes with 2-aminobenzothiazole derivatives. J Mol Struct. 2014;1063:160-169.
11. Synthesis and Characterisation of Novel Tetra dentate Schiff base Complexes: Biological Evaluation Exploring Anticancer Activity towards MCF 7 Cell Breast Cancer lines with in vitro Docking Studies. Indian J Chem. 2022;61(9).
12. Abdul-Rida NA, Talib KM. New Chalcone Derivatives as Anticancer and Antioxidant Agents: Synthesis, Molecular Docking Study And Biological Evaluation. Chemical Problems. 2024;22(2):177-186.
13. Hamzah SK, Jabbar NK, Almzaiel AJ, sabit RA. The Role Caspase-8 and DNA Methylation in patients with Ovarian Cancer: Relationship with Oxidative Stress and Inflammation. Research Journal of Pharmacy and Technology. 2021:2676-2680.
14. Sakıyan I, Logoglu E, Arslan S, Sari N, Şakiyan N. Antimicrobial activities of N-(2-hydroxy-1-naphthalidene)-amino acid(glycine, alanine, phenylalanine, histidine, tryptophane) Schiff bases and their manganese(III) complexes. BioMetals. 2004;17(2):115-120.
15. Yeap G-Y, Heng B-T, Faradiana N, Zulkifly R, Ito MM, Tanabe M, et al. Synthesis, molecular structures and phase transition studies on benzothiazole-cored Schiff bases with their Cu(II) and Pd(II) complexes: Crystal structure of (E)-6-methoxy-2-(4-octyloxy-2-hydroxybenzylideneamino) benzothiazole. J Mol Struct. 2012;1012:1-11.
16. Ghozlojeh N, Setamdideh D. Synthesis of Oximes from the Corresponding of Organic Carbonyl Compounds with NH_2OH.HCl and Oxalic Acid. Oriental Journal of Chemistry. 2015;31(3):1823-1825.
17. Yernale NG, Udayagiri MD, Mruthyunjayaswam BHM. Synthesis, characterization, mass spectral fragmentation, thermal study and biological evaluation of new Schiff base ligand and its metal(II) complexes derived from 4-(diethylamino)salicylaldehyde and thiazole moiety. European Journal of Chemistry. 2016;7(1):56-65.
18. Jasim L, Radhy N, Jamel H. Synthesis and Characterization of Poly (Acryl Amide - Maleic Acid) Hydrogel: Adsorption Kinetics of a Malachite Green from Aqueous Solutions. Eurasian Journal of Analytical Chemistry. 2018;13(1b).
19. Jasim LS, Abdulsahib WK, Ganduh SH, Radia ND. New Approach for Sulfadiazine Toxicity Management using Carboxymethyl Cellulose Grafted Acrylamide Hydrogel. International Journal of Drug Delivery Technology. 2020;10(02):259-264.
20. Kareem Hamzah S. Study some biochemical parameters in pregnant women with hypertension. Journal of Physics: Conference Series. 2019;1234(1):012092.
21. One Pot Multicomponent Synthesis of Novel Thiazolopyrimidines. Chemical Science Transactions. 2018.
22. Adimurthy S, Ramachandraiah G, Bedekar AV, Ghosh S, Ranu BC, Ghosh PK. Eco-friendly and versatile brominating reagent prepared from a liquid bromine precursor. Green Chem. 2006;8(10):916.
23. Spectrophotometric Determination of Metoclopramide- HCl in the standard raw and it compared with pharmaceuticals. Journal of Pharmaceutical Negative Results. 2021;21(2).
24. Atyaa AI, Radhy ND, Jasim LS. Synthesis and Characterization of Graphene Oxide/Hydrogel Composites and Their Applications to Adsorptive Removal Congo Red from Aqueous Solution. Journal of Physics: Conference Series. 2019;1234(1):012095.
25. Mahmood Taher A, Ali Kadhim Kyhoiesh H, Shakir Waheeb A, Al-Adilee KJ, Jasim LS. Synthesis, characterization, biological activity, and modelling protein docking of divalent, trivalent, and tetravalent metal ion complexes of new azo dye ligand (N,N,O) derived from benzimidazole. Results in Chemistry. 2024;12:101911.
26. Bigdeli MA, Nikje MMA, Jafari S, Heravi MM. Regioselective Synthesis of syn-oximes using 3Å Molecular Sieves in a Solventless System. Journal of Chemical Research. 2002;2002(1):20-21.
27. Rahman A, Jonnalagadda SB. Swift and Selective Reduction of Nitroaromatics to Aromatic Amines with Ni–Boride–Silica Catalysts System at Low Temperature. Catal Lett. 2008;123(3-4):264-268.
28. Sharghi H, Sarvari MH. Selective Synthesis of E and Z Isomers of Oximes. Synlett. 2001;2001(01):0099-0101.
29. Ali Bawa R, Mohammed Friwan M. Synthesis of Some Acetophenone Oximes and Their Corresponding Bridged Terphthaloyl Oxime Esters. Academic Journal of Life Sciences. 2019(511):87-92.
30. Qazi SJS, Rennie AR, Cockcroft JK, Vickers M. Use of wide-angle X-ray diffraction to measure shape and size of dispersed colloidal particles. Journal of Colloid and Interface Science. 2009;338(1):105-110.
31. Demina MM, Novopashin PS, Sarapulova GI, Afonin AV, Tikhonov AY, Medvedeva AS. Reaction of 3-trimethylsilylprop-2-ynal with α-hydroxyamino oximes. Russ J Org Chem. 2007;43(4):507-510.
32. Ghurab MS, El-Gammal OA, El-Gamil MM, Abu El-Reash GM. Preparation, investigation, DFT, pH-metric and cyclic voltammetry of Cr(III), Fe(III), Co(II), Ni(II) and Cu(II) complexes derived from 2-(2-((2Z,3Z)-3-(hydroxyimino) butan-2-ylidene) hydrazineyl)-2-oxo-N-(pyridin-2-yl) acetamide (H3BYPA) and evaluation of their biological activity. J Mol Struct. 2023;1272:134156.
33. Duc DX, Dung VC. Microwave-assisted, [Bmim]HSO4-catalyzed the Friedländer Quinoline Synthesis of Quinoline Under Solvent-free Conditions. Current Organocatalysis. 2022;9(2):117-123.
34. Synthesis, Characterization, Antifungal and Insecticidal Studies of Some Thiocyanato-Bridged Bimetallic Complexes Containing Ni(II), Cd(II), Hg(II) and N, N'-Bis(benzylidene) 1, 2-phenylenediamine Schiff Base. Chemical Science Transactions. 2013;2(4).
35. Şahin Ö, Özdemir ÜÖ, Seferoğlu N, Genc ZK, Kaya K, Aydıner B, et al. New platinum (II) and palladium (II) complexes of coumarin-thiazole Schiff base with a fluorescent chemosensor properties: Synthesis, spectroscopic characterization, X-ray structure determination, in vitro anticancer activity on various human carcinoma cell lines and computational studies. J Photochem Photobiol B: Biol. 2018;178:428-439.
36. Bayramov A. Environmental Regionalism in the Caspian Sea: A Functionalist Approach. Globalizing Regionalism and International Relations: Policy Press; 2021. p. 103-124.
37. Mahde BW, Sultan AM, Mahdi MA, Jasim LS. Kinetic Adsorption and Release Study of Sulfadiazine Hydrochloride

Drug from Aqueous Solutions on GO/P(AA-AM-MCC) Composite. INTERNATIONAL JOURNAL OF DRUG DELIVERY TECHNOLOGY. 2022;12(04):1583-1589.

38. Siregar AH, Setyawan BA, Marasabessy A. Flame retardant properties of composite fiberglass reinforced unsaturated polyester resin. AIP Conference Proceedings: Author(s); 2018. p. 050007.
39. Koyama E, Yang G, Tsuzuki S, Hiratani K. Synthesis of Novel Bis(benzoxazole) Derivatives by Tandem Claisen Rearrangement and Their Fluorescence Behavior. European Journal of Organic Chemistry. 2002;2002(12):1996.
40. Netalkar PP, Netalkar SP, Budagumpi S, Revankar VK. Synthesis, crystal structures and characterization of late first row transition metal complexes derived from benzothiazole core: Anti-tuberculosis activity and special emphasis on DNA binding and cleavage property. Eur J Med Chem. 2014;79:47-56.
41. Sahib IJ, Aljeboree AM, Mahdi AB, Jasim LS, Alkaim AF. Highly efficient removal of toxic Pb(II) from aqueous solution by chitosan-g-p(AA-co-AAm) hydrogel: Kinetic, models. AIP Conference Proceedings: AIP Publishing; 2023. p. 040073.
42. Sattar R, Mukhtar R, Atif M, Hasnain M, Irfan A. Synthetic transformations and biological screening of benzoxazole derivatives: A review. J Heterocycl Chem. 2020;57(5):2079-2107.
43. Mahdi MA, Oroumi G, Samimi F, Dawi EA, Abed MJ, Alzaidy AH, et al. Tailoring the innovative Lu2CrMnO6 double perovskite nanostructure as an efficient electrode materials for electrochemical hydrogen storage application. Journal of Energy Storage. 2024;88:111660.
44. Sajeesh S, Sharma CP. Mucoadhesive hydrogel microparticles based on poly (methacrylic acid-vinyl pyrrolidone)-chitosan for oral drug delivery. Drug Deliv. 2010;18(4):227-235.
45. Kianipour S, Razavi FS, Hajizadeh-Oghaz M, Abdulsahib WK, Mahdi MA, Jasim LS, et al. The synthesis of the P/N-type $NdCoO_3/g-C_3N_4$ nano-heterojunction as a high-performance photocatalyst for the enhanced photocatalytic degradation of pollutants under visible-light irradiation. Arabian Journal of Chemistry. 2022;15(6):103840.
46. Hosseini M, Ghanbari M, Dawi EA, Mahdi MA, Ganduh SH, Jasim LS, et al. Investigations of nickel silicate for degradation of water-soluble organic pollutants. Int J Hydrogen Energy. 2024;61:307-315.
47. McAfee L. Infrared and Raman Spectra of Inorganic and Coordination Compounds. Part A: Theory and Applications in Inorganic Chemistry; Part B: Application in Coordination, Organometallic, and Bioinorganic Chemistry, 5th Edition (Nakamoto, Kazuo). J Chem Educ. 2000;77(9):1122.
48. Chi Y, Chou P-T. Transition-metal phosphors with cyclometalating ligands: fundamentals and applications. Chem Soc Rev. 2010;39(2):638-655.
49. Barfeie H, Grivani G, Eigner V, Dusek M, Khalaji AD. Copper(II), nickel(II), zinc(II) and vanadium(IV) Schiff base complexes: Synthesis, characterization, crystal structure determination, and thermal studies. Polyhedron. 2018;146:19-25.
50. El-Sonbati AZ, Diab MA, El-Bindary AA, Mohamed GG, Morgan SM, Abou-Dobara MI, et al. Geometrical structures, thermal stability and antimicrobial activity of Schiff base supramolecular and its metal complexes. J Mol Liq. 2016;215:423-442.
51. Batool M, Haider MN, Javed T. Applications of Spectroscopic Techniques for Characterization of Polymer Nanocomposite: A Review. Journal of Inorganic and Organometallic Polymers and Materials. 2022;32(12):4478-4503.
52. Majeed HJ, Idrees TJ, Mahdi MA, Abed MJ, Batool M, Yousefi SR, et al. Synthesis and application of novel sodium carboxy methyl cellulose-g-poly acrylic acid carbon dots hydrogel nanocomposite (NaCMC-g-PAAc/ CDs) for adsorptive removal of malachite green dye. Desalination and Water Treatment. 2024;320:100822.
53. Shah A, Arjunan A, Manning G, Batool M, Zakharova J, Hawkins AJ, et al. Sequential novel use of Moringa oleifera Lam., biochar, and sand to remove turbidity, E. coli, and heavy metals from drinking water. Cleaner Water. 2024;2:100050.
54. Afanou KA, Straumfors A, Skogstad A, Skaar I, Hjeljord L, Skare Ø, et al. Profile and Morphology of Fungal Aerosols Characterized by Field Emission Scanning Electron Microscopy (FESEM). Aerosol Sci Technol. 2015;49(6):423-435.
55. Jamel HO, Jasim MH, Mahdi MA, Ganduh SH, Batool M, Jasim LS, et al. Adsorption of Rhodamine B dye from solution using 3-((1-(4-((1H-benzo[d]imidazol-2-yl)amino) phenyl)ethylidene)amino)phenol (BIAPEHB)/ P(AA-co-AM) composite. Desalination and Water Treatment. 2025;321:101019.
56. Neupane U, Rai US, Rai RN. Thermal, physicochemical and spectroscopic studies on some novel organic complexes obtained by green synthesis. J Therm Anal Calorim. 2018;132(3):1741-1752.
57. Iacopetta D, Ceramella J, Baldino N, Sinicropi M, Catalano A. Targeting Breast Cancer: An Overlook on Current Strategies. Int J Mol Sci. 2023;24(4):3643.
58. Kumar N, Mangla M. Nanotechnology and nanobots unleashed: pioneering a new era in gynecological cancer management – a comprehensive review. Cancer Chemother Pharmacol. 2025;95(1).